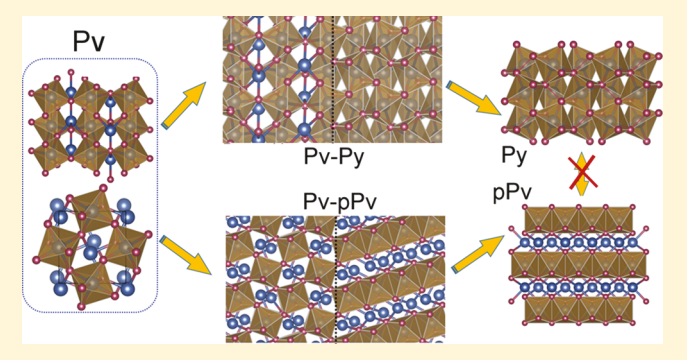
pubs.acs.org/IC

# Structure-Controlled Oxygen Concentration in Fe<sub>2</sub>O<sub>3</sub> and FeO<sub>2</sub>

Sheng-cai Zhu, †,‡,¶ Jin Liu, §,¶ Qingyang Hu,\*,‡ Wendy L. Mao, Yue Meng, Dongzhou Zhang, Ho-kwang Mao, ‡,# and Qiang Zhu\*,†

Supporting Information

ABSTRACT: Solid-solid reaction, particularly in the Fe-O binary system, has been extensively studied in the past decades because of its various applications in chemistry and materials and earth sciences. The recently synthesized pyrite-FeO<sub>2</sub> at high pressure suggested a novel oxygen-rich stoichiometry that extends the achievable O-Fe ratio in iron oxides by 33%. Although FeO2 was synthesized from Fe<sub>2</sub>O<sub>3</sub> and O<sub>2</sub>, the underlying solid reaction mechanism remains unclear. Herein, combining in situ X-ray diffraction experiments and first-principles calculations, we identified that two competing phase transitions starting from Fe<sub>2</sub>O<sub>3</sub>: (1) without O<sub>2</sub>, perovskite-Fe<sub>2</sub>O<sub>3</sub> transits to the post-perovskite



structure above 50 GPa; (2) if free oxygen is present, O diffuses into the perovskite-type lattice of Fe<sub>2</sub>O<sub>3</sub> leading to the pyritetype FeO2 phase. We found the O-O bonds in FeO2 are formed by the insertion of oxygen into the Pv lattice via the external stress and such O-O bonding is only kinetically stable under high pressure. This may provide a general mechanism of adding extra oxygen to previous known O saturated oxides to produce unconventional stoichiometries. Our results also shed light on how O is enriched in mantle minerals under pressure.

## 1. INTRODUCTION

Oxygen-rich (peroxides and superoxides) materials are often found in alkali metal oxides or alkaline-earth metal oxides because of the small cation to anion radius ratio at ambient pressure. Because of the fragile O-O bonds, the peroxides  $[O_2]^{2-}$  and superoxides  $[O_2]^{-}$  species are often metastable and prone to release O and form stable oxides at ambient conditions, making them widely used as decolorizers and aerophores in our daily life. External pressure can alter the ionic radius,2 stiffen bonds, and thus give rise to thermal stability of oxygen-rich materials, such as LiO2, MgO2, 4,5 and FeO2.6 These phenomena may have great implications in materials sciences and planetary sciences. For example, MgO<sub>2</sub> peroxides are predicted to exist as planet forming materials under strong oxidizing conditions.

Iron oxides are major naturally occurring compounds in the earth and have a variety of industrial applications.<sup>7,8</sup> Seeking new iron oxides with different valence and spin states of iron has been a long-term interest for both materials scientists and

geoscientists. To date, besides the common stoichiometry of FeO, Fe<sub>3</sub>O<sub>4</sub>, and Fe<sub>2</sub>O<sub>3</sub>, several novel stable iron oxides such as  $\operatorname{Fe_4O_5}^9$   $\operatorname{Fe_5O_6}^{10}$  and  $\operatorname{Fe_5O_7}^{11}$  have been reported under various pressure-temperature conditions. All these newly discovered iron oxides are regarded as mixed-valence oxides, falling into the stoichiometry range between FeO and Fe<sub>2</sub>O<sub>3</sub>. Most of them can be actually considered as the homologous series of  $n\text{FeO} \cdot m\text{Fe}_2\text{O}_3$ . Given the abundance of both Fe and O, their chemistries play a critical role in redox equilibria of the solid earth, which thus in turn affect the oxygen fugacity, chemical differentiation, and physical properties.

Along this track, it was reported that iron could be oxidized further beyond Fe<sub>2</sub>O<sub>3</sub>, similar to what happened on alkali and alkali-earth metals. Indeed, the pyrite-type FeO<sub>2</sub> (denoted as Py-FeO<sub>2</sub>) was synthesized from the mixture of Fe<sub>2</sub>O<sub>3</sub> and O<sub>2</sub> at 74 GPa and 1700 K, which has the highest O concentration in

Received: September 27, 2018 Published: December 17, 2018



<sup>&</sup>lt;sup>†</sup>Department of Physics and Astronomy, High Pressure Science and Engineering Center, University of Nevada, Las Vegas, Nevada 89154, United States

<sup>&</sup>lt;sup>‡</sup>Center for High Pressure Science and Technology Advanced Research (HPSTAR), Shanghai 201203, P. R. China

<sup>§</sup>Department of Geological Sciences, Stanford University, Stanford, California 94305, United States

Hawai'i Institute of Geophysics and Planetology, School of Ocean and Earth Science and Technology, University of Hawai'i at Manoa, Honolulu, Hawaii 96822, United States

<sup>&</sup>lt;sup>1</sup>High Pressure Collaborative Access Team, X-ray Science Division, Argonne National Laboratory, Argonne, Illinois 60439, United

Geophysical Laboratory, Carnegie Institution of Washington, Washington, D.C. 20015, United States

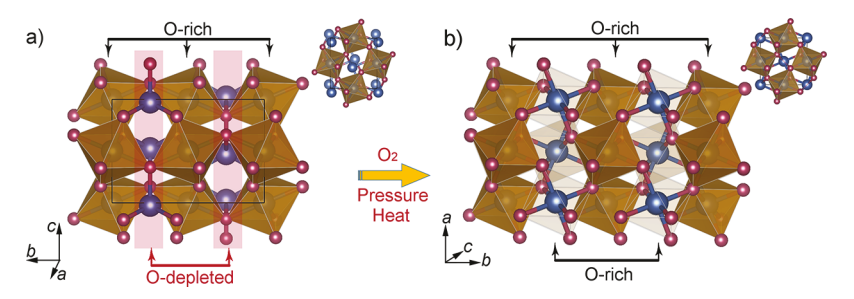


Figure 1. Atomic structure of (a) Pv-Fe $_2O_3$  and (b) Py-Fe $O_2$ , the inset is top view from Pv(010) and Py(010). The similar arrangement of Fe and O in Py-Fe $O_2$  and Pv-Fe $O_3$  indicates that they may form a low-energy interface. Red: O, blue: Fe.

all known iron oxides.<sup>6</sup> The Py-FeO<sub>2</sub> bears O–O bonding<sup>6,12,13</sup> and is only stable at high pressure. Similar to many peroxides, it becomes unstable upon decompression and releases O<sub>2</sub>.<sup>6</sup> For example, below 40 GPa, Py-FeO<sub>2</sub> starts to degas oxygen and reverts to Fe<sub>2</sub>O<sub>3</sub>. While the thermodynamic phase stability fields for Fe<sub>2</sub>O<sub>3</sub><sup>14–17</sup> and FeO<sub>2</sub><sup>6,18,19</sup> have been extensively investigated, the general structure modification mechanism involving stoichiometric variation remains elusive. The kinetics in the oxygenation reaction is fundamentally important to understand how they are stabilized at high pressure. This motivated us to perform a detailed investigation on the atomistic mechanism in the oxygenation reaction from Fe<sub>2</sub>O<sub>3</sub> to Py-FeO<sub>2</sub> and study how this reaction competes against polymorphic phase transitions to other high-pressure forms of Fe<sub>2</sub>O<sub>3</sub>.

# 2. RESULTS

# 2.1. Density Functional Theory Calculation Results.

The key to understand the solid—solid reaction is to establish the structural relation between Fe<sub>2</sub>O<sub>3</sub> and FeO<sub>2</sub> and construct the reaction interface for the O diffusion. Among the many high-pressure polymorphs of Fe<sub>2</sub>O<sub>3</sub>, including hematite phase (α-Fe<sub>2</sub>O<sub>3</sub>), Rh<sub>2</sub>O<sub>3</sub>-II-type, perovskite-type (Pv-Fe<sub>2</sub>O<sub>3</sub>), postperovskite-type (pPv-Fe<sub>2</sub>O<sub>3</sub>) and *Aba*2-type, we found that the Pv-Fe<sub>2</sub>O<sub>3</sub> shares fairly strong structural similarity with Py-FeO<sub>2</sub> (see Supporting Information Figure S1 for details). On the basis of the available data, the Pv-type phase is only thermodynamically stable within a narrow pressure window of 45–50 GPa and transforms to the pPv phase above 50 GPa upon heating. <sup>15,16</sup> It was also reported that Pv-Fe<sub>2</sub>O<sub>3</sub> is slightly triclinic distorted<sup>20</sup> but this would not be considered in this study.

Pv-Fe<sub>2</sub>O<sub>3</sub> has an orthorhombic unit cell (*Pnma*, no. 62) which contains two different Fe cation sites. Using the prototypical ABO<sub>3</sub> structure for the Pv-structure, Fe cations at A sites fill the interstices of 8 Fe–O-octahedral and hold 4 short Fe–O bonds of ~1.87 Å, 2 long Fe–O bonds of ~2.22 Å, and 2 even longer bonds of ~2.45 Å at 75 GPa. In light of the first shell of the Fe–O, the A site layer corresponds to a FeO formula, <sup>21</sup> thus labeled as the *O*-depleted layer. Meanwhile, Fe cations in the B site fill the O octahedral interstices (all the Fe–O bonds are ~1.86 Å) that correspond to a FeO<sub>2</sub> formula, denoted as the *O*-rich layer. In the Pv-Fe<sub>2</sub>O<sub>3</sub> structure, the shortest O···O distance is 2.52 Å. The *O*-rich and the *O*-depleted layers are alternating along the [010] direction, leading to the stoichiometry of Fe<sub>2</sub>O<sub>3</sub>.

In FeO<sub>2</sub> (*Pa3*, no. 205), all Fe atoms fill the octahedral sites, thus making them fully *O*-rich layers. Each O is shared by 3 [FeO<sub>6</sub>] octahedral and connected with a neighboring O in the O–O bond. The O–O bond length is 1.9 Å from the

experiment at 76 GPa and is estimated as ~1.8 Å according to theoretical calculations with Hubbard part U=5 eV (~1.9 Å when U=4 eV) at 75 GPa. <sup>12,13</sup> The structure of FeO<sub>2</sub> is analogical to a certain group of peroxides (e.g., pyrite-MgO<sub>2</sub>) and dioxides (e.g. PdF<sub>2</sub>-type SiO<sub>2</sub>). Although the O–O bond length in FeO<sub>2</sub> is larger than values of 1.29–1.53 Å in typical peroxides, <sup>1</sup> both experiment and theory suggest an unusual O–O bonding in FeO<sub>2</sub> (see the electron localization function map in Figure S2 in Supporting Information). Therefore, we regard FeO<sub>2</sub> as the pyrite-type phase. <sup>22</sup>

From the top view,  $Py\text{-FeO}_2$  and the O-rich layers of  $Pv\text{-Fe}_2O_3$  have the same atomic arrangement (insets in Figure 1). However, Fe atoms of  $Fe_2O_3$  in the O-depleted layer are positioned at different sites, thus distinguishing two structures. Once all the O-depleted layers in  $Pv\text{-Fe}_2O_3$  are filled by O, they will turn to O-rich layers and transform to  $Py\text{-FeO}_2$ .

On the basis of this structural relation, we constructed an interface model between the (010) plane of Py-FeO<sub>2</sub> and the (010) plane of Pv-Fe<sub>2</sub>O<sub>3</sub>, namely,  $(010)_{p_v}//(010)_{p_v}$  +  $[100]_{Pv}/[100]_{Pv}$ . Its stability can be assessed by the interfacial energy  $\gamma$  via first-principles calculation. We defined interface energy  $\gamma$  as  $\gamma = (E_{a/b} - E_a - E_b)/2S$ , where S is the interfacial area,  $E_a$  and  $E_b$  are the energies of the pure phases, and  $E_{a/b}$  is the energy of the mixed phase in a supercell containing two equivalent interfaces under periodic boundary conditions.<sup>23</sup> To describe localized 3d electrons of Fe, we used the DFT + U scheme<sup>24</sup> with a *U* value of 5.0 eV following a previous work.<sup>25</sup> The on-site U parameter may change the total energy for each individual structure but will have limited effects on the energy barrier and interface energy. Our calculation enabled spin polarization, and the structures were relaxed for atomic forces. In our calculation, both Pv-Fe<sub>2</sub>O<sub>3</sub> and pPv-Fe<sub>2</sub>O<sub>3</sub> have mixed high-spin and low-spin states. Different spin states are alternately aligned along the [010] direction for Pv and the [001] direction for pPv as were described in the ref 26. The Fe atoms in Py-FeO2 are in the low spin-state. For the magnetic structure, both Pv-Fe<sub>2</sub>O<sub>3</sub> and pPv-Fe<sub>2</sub>O<sub>3</sub> structures are treated as antiferromagnetic configuration, while FeO<sub>2</sub> is nonmagnetic. The magnetization at the interface is extremely complex. After geometric relaxation, we managed to optimize the interface supercell to a local minimum. For this relaxed structure, Fe atoms at the reaction interface form a pseudo antiferromagnetic configuration (see Figure S3 in Supporting Information), with Fe atoms of the Py-phase further away from the interface staying nonmagnetic. After optimization, the interface energy value is calculated as 0.53 J/m<sup>2</sup> at 75 GPa. This is considered as a low-energy interface compared with many other welldefined systems. For example, the rutile (101)/anatase (112) has an interface energy of 1.49 J/m<sup>2</sup> because of the pronounced lattice mismatch,<sup>27</sup> and the interface energy of

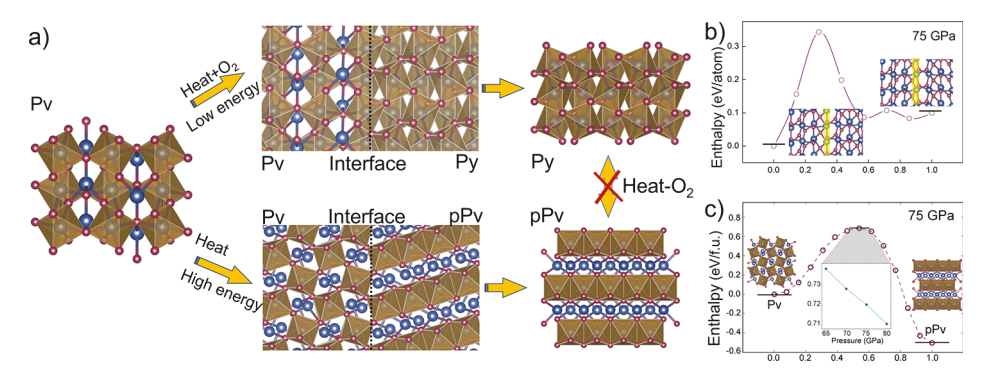


Figure 2. Kinetics of O diffusion and Pv-to-pPv phase transition in  $Fe_2O_3$ . (a) Py-FeO<sub>2</sub> and Pv-Fe<sub>2</sub>O<sub>3</sub> interface with oxygen diffusion (upper panel) and the interface for the phase transition from Pv-Fe<sub>2</sub>O<sub>3</sub> to pPv-Fe<sub>2</sub>O<sub>3</sub> (bottom panel). (b) Enthalpy barrier for O diffusion at 75 GPa; (c) transition path from Pv-Fe<sub>2</sub>O<sub>3</sub> to pPv-Fe<sub>2</sub>O<sub>3</sub> from the ssNEB method; no direct path between pPv-Fe<sub>2</sub>O<sub>3</sub> and Py-FeO<sub>2</sub> can be found.

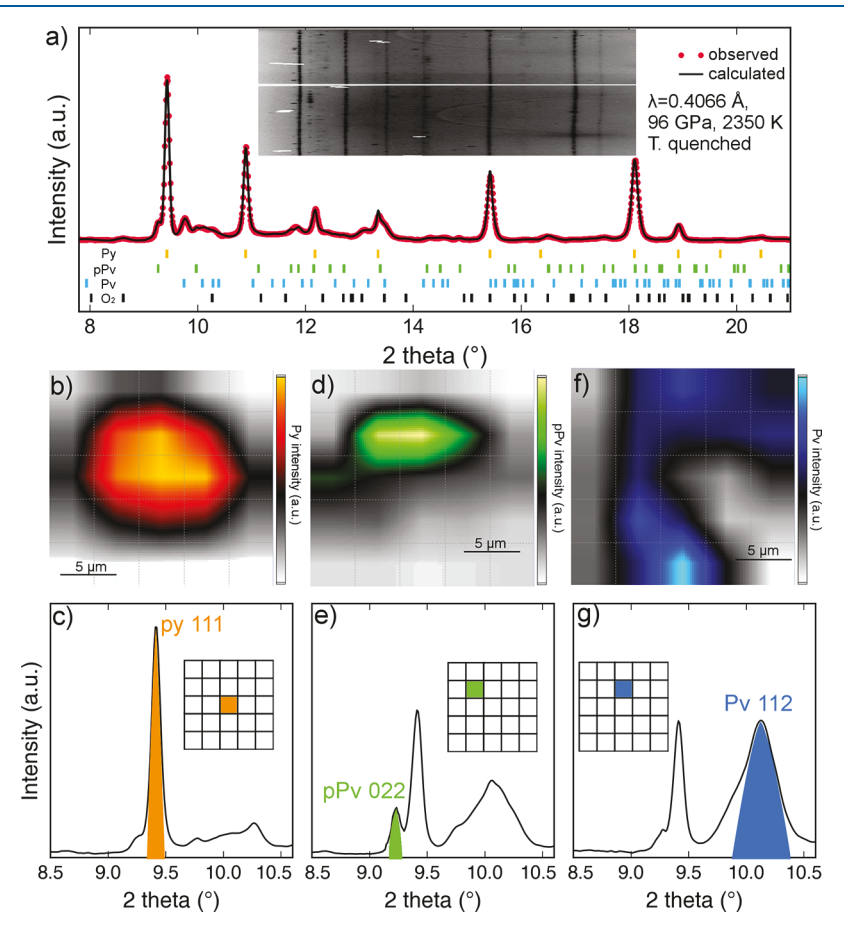


Figure 3. XRD mapping of synthesized  $FeO_2$  at 96 GPa. (a) Fully indexed  $Py-FeO_2$  at the heating center. The O-O distance is 1.87 Å. The inset is the caked diffraction pattern. (b-g). Distributions of  $Py-FeO_2$ ,  $pPv-Fe_2O_3$ , and  $Pv-Fe_2O_3$  are characterized by the intensities of their signature 111, 022, and 112 peaks, respectively. Double-sided heating laser spots generally cover all the sample region and thermal gradient is estimated up to 200 K. The dominant  $Py-FeO_2$  at the heating center is fitted by the Rietveld method, while the rest spotty peaks from  $Fe_2O_3$  and  $O_2$  are analyzed by LeBail fitting. The final refinement factors are  $R_1 = 0.069$ ,  $wR_2 = 0.14$ . The O-O distance is 1.87 Å for reference only. Lattice parameters are reported in Supporting Information, Table S1.

the symmetric  $\Sigma 3(110)$  grain boundary in silicon is 0.76 J/m². Therefore, we conclude that such an interface is energetically favorable under high pressure conditions. It is worth mentioning that  $Rh_2O_3\text{-II-type}$  phase is close to Pv-Fe $_2O_3$  in the atomic structure and also form reaction interface with the pyrite phase (see Figure S5). However, the  $Rh_2O_3\text{-II}$  type phase transforms to Pv phase with a shallow energy barrier (e.g., 0.019 eV/f.u. at 65 GPa) when pressure is greater than 45 GPa. Therefore,  $Rh_2O_3\text{-II-type}$  Fe $_2O_3$  is kinetically

unstable even at 300 K and 75 GPa. Moreover, a direct interface of  $Rh_2O_3$ -II/Py leads to a much higher interface energy (0.922 J/m²). This is consistent with our high-pressure experiment (>75 GPa) that Pv-Fe<sub>2</sub>O<sub>3</sub> is the preferred phase to react with O<sub>2</sub>.

The satisfactory atomic match between  $(010)_{Py}$  and  $(010)_{Py}$  provides the O diffusion channel for the oxygenation process. Mimicking O diffusion, moving the O atom from the *O*-rich to *O*-depleted layer only overcomes a tiny energy barrier of 0.34

eV per atom (equivalent to 0.032 eV/Ų) at 75 GPa by the nudged elastic band (NEB) method. In this process, the *O*-rich layer transits to the *O*-depleted layer, while the rest of the structure remains unchanged. This ensures that the frame structure can be retained during O diffusion. Owing to the relatively small kinetic barrier, it is safe to say that Pv-Fe<sub>2</sub>O<sub>3</sub> readily transforms to the Py-FeO<sub>2</sub> phase when free O atoms are present.

At the same pressure range (>50 GPa), Pv-Fe<sub>2</sub>O<sub>3</sub> transforms to the polymorphic pPv-Fe<sub>2</sub>O<sub>3</sub> when O<sub>2</sub> is depleted. 11,14 It is generally believed that the archetypal Pv to pPv transition requires a rather high activation energy barrier.<sup>31</sup> Here, we explore the Pv-to-pPv Fe2O3 phase transition pathways by an alternative sampling scheme, namely, stochastic surface walking (SSW) pathway method<sup>32,33</sup> (details in the Method section). SSW produced the most kinetically favored phase transition pathway which was further optimized by the solidstate NEB method (ssNEB), 30 variable-cell NEB (VC-NEB), 34 and variable-cell double-ended surface walking (VC-DESW)35 method. As shown in Figure 2a, by shearing along the [100] direction, Pv-Fe<sub>2</sub>O<sub>3</sub> transforms to pPv-Fe<sub>2</sub>O<sub>3</sub> with an enthalpy barrier 0.69 eV/f.u. from ssNEB (similarly 0.68 eV/f.u. for VC-NEB and 0.72 eV/f.u. for VC-DESW), equivalent to 0.046 eV/  $Å^2$ , at 75 GPa. The high energy barrier is consistent with the experimental observation that Pv-to-pPv phase transition only takes place as high as 2000-2320 K as Ono and Ohishi reported. 16 Pv-pPv transitions in bridgmanite MgSiO<sub>3</sub> was proposed to follow a stacking fault mechanism by Oganov et al.<sup>31</sup> and it was confirmed by Tschauner through an experiment.<sup>36</sup> Here, we found that the phase transition between Pv- and pPv-Fe<sub>2</sub>O<sub>3</sub> followed the same mechanism. Using the finite strain theory,<sup>37</sup> we derived that the phase transition orientation relation is  $(001)_{Pv}//(110)_{pPv}$  + [010]<sub>Pv</sub>//[001]<sub>pPv</sub>. Figure 2a shows a supercell interface model following this relation. Its interface energy is 0.38 J/ m<sup>2</sup> after full optimization, which is smaller than the interface of  $(010)_{P_V}//(010)_{P_V} + [100]_{P_V}/[100]_{P_V}$ . Comparing with the O diffusion in Py-FeO2, the structure phase transition to pPv-Fe<sub>2</sub>O<sub>3</sub> forms a same stable reaction interface as Py but overcomes a much higher energy barrier than Pv to Py.

**2.2. In Situ High-Pressure Experiment.** To confirm our hypothesis, we investigated the solid reaction pathways by in situ synchrotron X-ray diffraction (XRD) experiments. We compressed a piece of Fe<sub>2</sub>O<sub>3</sub> in O<sub>2</sub> pressure medium to 90 GPa and heated it by laser (Supporting Information Figure S4). In Figure 3a, intensities of Py-FeO<sub>2</sub> diffraction gradually increased under around 2350 K laser heating and FeO<sub>2</sub> pattern eventually overwhelms all other Fe<sub>2</sub>O<sub>3</sub> phase's after 30 min heating. Pressure equilibrated at 96 GPa after quenching to room temperature. At the center of heating area (Figure 3a), strong and smooth powder diffraction peaks are readily indexed for Py-FeO2 using the Rietveld method while minor residual spotty peaks are associated with Fe<sub>2</sub>O<sub>3</sub> and  $\varepsilon$ -O<sub>2</sub>. The final refinement factors are  $R_1 = 0.069$  and  $wR_2 = 0.14$ . The O-O distance is 1.87 Å that falls between traditional peroxide and PdF2-dioxide. Figure 3b-g shows the 2 dimensional XRD mapping over the heated sample. In the spatial view, we can find that both Py-FeO2 and pPv-Fe2O3 are contingent with the Pv-Fe<sub>2</sub>O<sub>3</sub>. Py-FeO<sub>2</sub> is the dominant phase among the coexistence of py-FeO2 and Pv- and pPv-Fe2O3, indicating that the phase transition to the Py-FeO<sub>2</sub> is kinetically favored. In our previous experiment, we did not attempt to associate any diffraction peaks with Pv-Fe<sub>2</sub>O<sub>3</sub> because it is considered as

a low-pressure phase.<sup>6</sup> However, because of the kinetics of the two competing phase transitions, the polymorphic transition to  $pPv-Fe_2O_3$  may be hindered by its higher energy barrier. As a result, the  $Pv-Fe_2O_3$  appears as a metastable interfacial structure in the mixed products even if the pressure is 75 GPa.

We further studied the kinetics of Pv-Fe<sub>2</sub>O<sub>3</sub> to Py-FeO<sub>2</sub> and polymorphic transition to pPv-Fe<sub>2</sub>O<sub>3</sub> by the time-dependent XRD analysis; see Figure 4. XRD patterns were collected at 96

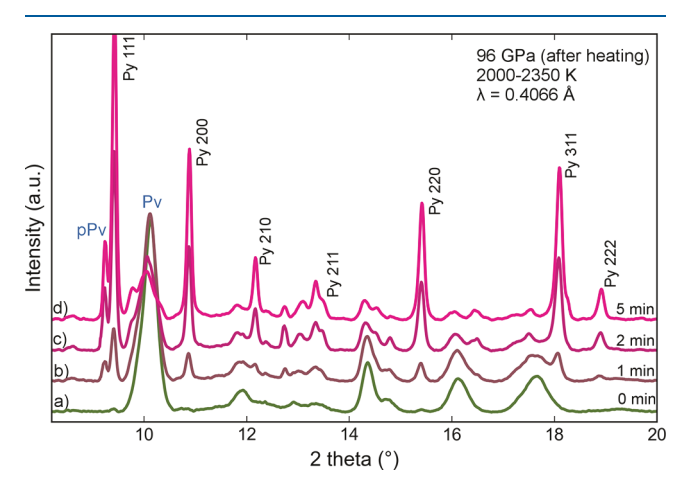


**Figure 4.** Time-resolved XRD patterns for a high-pressure sample during laser heating. All patterns were collected after heating for a certain amount of time and quenched to 300 K. (a) Before heating (0 min), (b) after 1 min heating, both Py-FeO<sub>2</sub> and pPv-Fe<sub>2</sub>O<sub>3</sub> were found in the heating center; (c,d) after 2 and 5 min heating, Pv-Fe<sub>2</sub>O<sub>3</sub> gradually transforms to Py-FeO<sub>2</sub> and pPv-Fe<sub>2</sub>O<sub>3</sub>. The reaction rate to Py-FeO<sub>2</sub> is faster than to pPv-Fe<sub>2</sub>O<sub>3</sub>. Each pattern was collected after 10 s X-ray exposure time. The pressure is measured after temperature quench with an uncertainty of  $\pm 2$  GPa; X-ray wavelength is 0.4066 Å.

GPa and quenched room temperature after heating at 2000–2350 K for a certain amount of time. Comparing the peak intensity of Py- and pPv-phase, the transition of Pv to Py phase has clearly higher productivity. The low productivity of pPv-Fe<sub>2</sub>O<sub>3</sub> is reproduced in another experimental run, where nearly pure Py-FeO<sub>2</sub> was found within the heating area (Supporting Information, Figure S5). According to the time-dependent XRD data, transition to Py-FeO<sub>2</sub> has a priority over Pv-Fe<sub>2</sub>O<sub>3</sub> when O is present.

To trace the degassing process, the sample was decompressed from high-pressure at ambient temperature. We decrease the pressure slowly and trace the products by XRD. As shown in Figure 5, while the diffraction intensities from Py-FeO<sub>2</sub> attenuate by releasing pressure, signals from Pv-Fe<sub>2</sub>O<sub>3</sub> stay strong. This is due to the reverse reaction by depleting O from Py-FeO<sub>2</sub> crystals. Because FeO<sub>2</sub> and Pv-Fe<sub>2</sub>O<sub>3</sub> form a well-matched reaction interface, a small portion of FeO<sub>2</sub> will transform back to Pv-Fe<sub>2</sub>O<sub>3</sub> without destroying the crystal framework. Below 46 GPa, the Pv-Fe<sub>2</sub>O<sub>3</sub> slips out of its stability field and started to fade away. At 31 GPa, the sample completely decomposed to  $\alpha$ -Fe<sub>2</sub>O<sub>3</sub>. Degassing of oxygen indicates that O–O bonds become fragile upon releasing pressure.

#### 3. DISCUSSION

The chemical reaction of  $2\text{Fe}_2\text{O}_3 + \text{O}_2 = 4\text{Fe}\text{O}_2$  is only observed at high pressure. After filling the *O*-depleted layer with O atoms, the original Pv-Fe<sub>2</sub>O<sub>3</sub> lattice suffers considerable compressive stresses in both [100] and [001] directions,

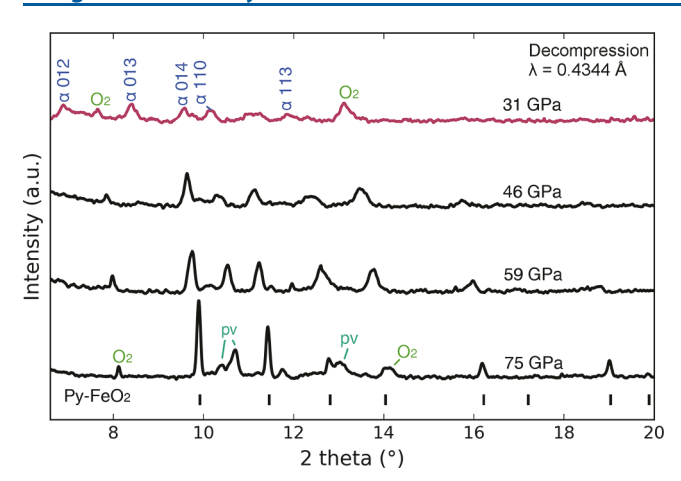


**Figure 5.** XRD pattern along the decompression process at 75, 59, 46, and 31 GPa. Signals from Py-FeO<sub>2</sub> become weak with decreasing pressure and eventually disappear at 31 GPa.

forcing the shortening of O–O length and eventually leading to the emergence of O–O pairs. As a result, O-depleted layers turn into O-rich layers and eventually form the Py-FeO $_2$  structure. On the other hand, the O–O bonds readily vanish by a reversible unpairing process. Decomposition of FeO $_2$  is ultimately triggered when the pyrite structure collapses upon releasing pressure. In a word, the O concentration changes in between Fe $_2$ O $_3$  and FeO $_2$  are largely due to the pressure effect, controlled by the atomistic structure.

The mechanism finds its most important application in the chemistry of earth's interiors. Although Fe<sub>2</sub>O<sub>3</sub> have many polymorphs, such as  $\alpha$ -Fe<sub>2</sub>O<sub>3</sub>,  $\iota$ -Fe<sub>2</sub>O<sub>3</sub>, Pv-Fe<sub>2</sub>O<sub>3</sub>, pPv-Fe<sub>2</sub>O<sub>3</sub>, and  $\theta$ -Fe<sub>2</sub>O<sub>3</sub>, our work found that only the phase transition between Pv and Py possesses such "switchable" characteristic. We did not observe similar reactions between any other Fe<sub>2</sub>O<sub>3</sub> polymorphs and Py-FeO<sub>2</sub>. This observation can be explained by the atomistic mechanism. Pv-Fe<sub>2</sub>O<sub>3</sub> and Py-FeO<sub>2</sub> have a strong structural relation, which provided them well-matched interface and low energy barrier. As a result, at the same pressure and temperature condition, the formation of Py-FeO<sub>2</sub> will be more favorable than the competing phase transition to pPv-Fe<sub>2</sub>O<sub>3</sub>. In other words, if the kinetic of Pv to pPv is more favorable than to Py, the transition of pPv-Fe<sub>2</sub>O<sub>3</sub> + O<sub>2</sub> to Py-FeO<sub>2</sub> would have to overcome a much higher energy barrier. Such transition kinetics may play a different role in the degassing or regassing of oxygen in earth's rocky materials.

It was reported that Py-FeO<sub>2</sub> can accumulate at earth's core—mantle boundary through iron—water reaction.  $^{38-40}$  The archetypal Pv structure in the simple form of ABO3 allows numerous cation combinations on the A and B sites, 41 creating an extraordinary Pv-type family. Replacing iron partially with other major earth's elements such as Mg or Al in Py-FeO2 can generate solid solution-like compounds of (Mg,Fe)O2 or (Al,Fe)O<sub>2</sub>. Indeed, hydrogen bearing pyrite-(Al,Fe)O<sub>2</sub> has been observed in the experiment by Zhang et al. 42 It provides important evidence that the pyrite phase can be a more viable material type in the earth. Therefore, the O diffusion mechanism between pyrite and perovskite structures in the current study can possibly apply to the materials in the general form of (Mg,Fe)(Al,Fe,Si)O<sub>3</sub> perovskite.<sup>43</sup> Although our current study only considers Fe and O, the alternating Orich and O-depleted layers in the perovskite structure have already provided the basis to apply this mechanism. Finding the appropriate pressure, temperature, and stoichiometry conditions to realize the Pv-to-Py phase transition in other minerals containing earth-abundant elements is the subject of future work. In addition to its geoscience implication, the Pv-to-Py reaction by adding extra oxygen to previous known O saturated oxides to produce unconventional stoichiometries may also apply to other materials, such as AlO<sub>2</sub> in the Al–O<sup>44</sup> system and GaO<sub>2</sub> in the Ga–O system. It would be a novel method to create a broader spectrum of O-rich materials that will have potential industrial applications.

#### 4. CONCLUSIONS

In summary, we establish an oxygenation mechanism between perovskite  $\text{Fe}_2\text{O}_3$  and pyrite  $\text{Fe}\text{O}_2$  in this work. Combining the first-principles calculation and in situ experiment, we identified that the most likely transition pathway is via O diffusion on the  $\text{Pv-Fe}_2\text{O}_3(010)$  and  $\text{Py-Fe}\text{O}_2(010)$  interface under high-pressure and oxygen-rich conditions. Thereby, we propose two competing phase transition pathways on  $\text{Fe}_2\text{O}_3$  controlled by its transforming structure: (1) polymorphic transition from  $\text{Pv-to}\ p\text{Pv-Fe}_2\text{O}_3$  when O is depleting and (2) oxygenation to  $\text{Py-Fe}\text{O}_2$  via O diffusion when excess  $\text{O}_2$  is present. The mechanisms may have great impact in understanding the oxygen enrichment in the interior of the earth.

#### ASSOCIATED CONTENT

## Supporting Information

The Supporting Information is available free of charge on the ACS Publications website at DOI: 10.1021/acs.inorg-chem.8b02764.

High-pressure in situ XRD experiment method; the calculation detail of SSW sampling method, the interface energy and O diffusion; the atomic structure of Py-FeO<sub>2</sub> and Fe<sub>2</sub>O<sub>3</sub> polymorphs; the electron localization function of MgO<sub>2</sub>, pyrite-type FeO<sub>2</sub>, and PdF<sub>2</sub>-type SiO<sub>2</sub> at 75 GPa; XRD pattern of reaction products of Pv-Fe<sub>2</sub>O<sub>3</sub> and oxygen at 75 GPa; and the Py-FeO<sub>2</sub> and Pv-Fe<sub>2</sub>O<sub>3</sub> interface and Py-FeO<sub>2</sub> and Rh<sub>2</sub>O<sub>3</sub>-II-type Fe<sub>2</sub>O<sub>3</sub> interface module (PDF)

## AUTHOR INFORMATION

## **Corresponding Authors**

\*E-mail: qingyang.hu@hpstar.ac.cn (Q.H.). \*E-mail: qiang.zhu@unlv.edu (Q.Z.).

#### ORCID

Sheng-cai Zhu: 0000-0003-3311-6723 Qingyang Hu: 0000-0002-2742-3017

# **Author Contributions**

<sup>¶</sup>S.-c.Z. and J.L. contributed equally.

#### **Notes**

The authors declare no competing financial interest.

#### ACKNOWLEDGMENTS

Work at UNLV is supported by the National Nuclear Security Administration under the Stewardship Science Academic Alliances program through DOE Cooperative Agreement DE-NA0001982. We acknowledge the use of computing resources from XSEDE and Center for Functional Nanomaterials under contract no. DE-AC02-98CH10086. A portion of simulation was conducted on the SR16000 facilities of the institute for Materials Research, Tohoku University. XRD was

conducted at the High Pressure Collaborative Access Team (HPCAT) and GeoSoilEnviroCARS (GSECARS), Advanced Photon Source, Argonne National Laboratory. HPCAT operation is supported by the DOE-NNSA under award number DE-NA0001974, with partial instrumentation funding by NSF. GSECARS is supported by the NSF-Earth Sciences (EAR-1634415) and DOE-Geosciences (DE-FG02-94ER14466). PX^2 program and the COMPRES-GSECARS gas loading system are supported by COMPRES under NSF Cooperative Agreement EAR-1661511. Y.M. acknowledges the support of DOE-BES/DMSE under award DE-FG02-99ER45775. S.-c.Z. and Q.H. are supported by NSFC (grant no: 21703004). W.L.M. and J.L. acknowledge support from the NSF (EAR-1446969). H.-k.M. is supported by the NSF (EAR-1345112, EAR-1722515, and EAR-1447438). HPSTAR is supported by NSAF (grant no: U1530402).

#### REFERENCES

- (1) Hoffman, C. W. W.; Ropp, R. C.; Mooney, R. W. Preparation, properties and structure of cadmium peroxide. *J. Am. Chem. Soc.* **1959**, *81*, 3830–3834.
- (2) Stavrou, E.; Yao, Y.; Goncharov, A. F.; Lobanov, S. S.; Zaug, J. M.; Liu, H.; Greenberg, E.; Prakapenka, V. B. Synthesis of xenon and iron-nickel intermetallic compounds at Earth's core thermodynamic conditions. *Phys. Rev. Lett.* **2018**, *120*, 096001.
- (3) Yang, W.; Kim, D. Y.; Yang, L.; Li, N.; Tang, L.; Amine, K.; Mao, H.-K. Oxygen-Rich Lithium Oxide Phases Formed at High Pressure for Potential Lithium-Air Battery Electrode. *Adv. Sci.* **2017**, *4*, 1600453.
- (4) Zhu, Q.; Oganov, A. R.; Lyakhov, A. O. Novel stable compounds in the Mg-O system under high pressure. *Phys. Chem. Chem. Phys.* **2013**, *15*, 7696–7700.
- (5) Lobanov, S. S.; Zhu, Q.; Holtgrewe, N.; Prescher, C.; Prakapenka, V. B.; Oganov, A. R.; Goncharov, A. F. Stable magnesium peroxide at high pressure. *Sci. Rep.* **2015**, *5*, 13582.
- (6) Hu, Q.; Kim, D. Y.; Yang, W.; Yang, L.; Meng, Y.; Zhang, L.; Mao, H.-K. FeO<sub>2</sub> and FeOOH under deep lower-mantle conditions and Earth's oxygen-hydrogen cycles. *Nature* **2016**, *534*, 241–244.
- (7) Zhou, X.; Xu, Q.; Lei, W.; Zhang, T.; Qi, X.; Liu, G.; Deng, K.; Yu, J. Origin of Tunable Photocatalytic Selectivity of Well-Defined  $\alpha$ -Fe2O3Nanocrystals. *Small* **2013**, *10*, 674–679.
- (8) Reddy, M. V.; Yu, T.; Sow, C. H.; Shen, Z. X.; Lim, C. T.; Subba Rao, G. V.; Chowdari, B. V. R.  $\alpha$ -Fe<sub>2</sub>O<sub>3</sub> Nanoflakes as an Anode Material for Li-Ion Batteries. *Adv. Funct. Mater.* **2007**, *17*, 2792–2799.
- (9) Lavina, B.; Dera, P.; Kim, E.; Meng, Y.; Downs, R. T.; Weck, P. F.; Sutton, S. R.; Zhao, Y. Discovery of the recoverable high-pressure iron oxide Fe<sub>4</sub>O<sub>5</sub>. *Proc. Natl. Acad. Sci. U.S.A.* **2011**, *108*, 17281–17285.
- (10) Lavina, B.; Meng, Y. Unraveling the complexity of iron oxides at high pressure and temperature: Synthesis of Fe<sub>5</sub>O<sub>6</sub>. Sci. Adv. 2015, 1, No. e1400260.
- (11) Bykova, E.; Dubrovinsky, L.; Dubrovinskaia, N.; Bykov, M.; McCammon, C.; Ovsyannikov, S. V.; Liermann, H.-P.; Kupenko, I.; Chumakov, A. I.; Rüffer, R.; Hanfland, M.; Prakapenka, V. Structural complexity of simple  $\text{Fe}_2\text{O}_3$  at high pressures and temperatures. *Nat. Commun.* **2016**, *7*, 10661.
- (12) Jang, B. G.; Kim, D. Y.; Shim, J. H. Metal-insulator transition and the role of electron correlation in FeO<sub>2</sub>. *Phys. Rev. B* **2017**, *95*, 075144
- (13) Streltsov, S. S.; Shorikov, A. O.; Skornyakov, S. L.; Poteryaev, A. I.; Khomskii, D. I. Unexpected 3+ valence of iron in FeO<sub>2</sub>, a geologically important material lying "in between" oxides and peroxides. *Sci. Rep.* **2017**, *7*, 13005.
- (14) Ono, S.; Kikegawa, T.; Ohishi, Y. High-pressure phase transition of hematite, Fe<sub>2</sub>O<sub>3</sub>. *J. Phys. Chem. Solids* **2004**, *65*, 1527–1530.

(15) Ono, S.; Funakoshi, K.; Ohishi, Y.; Takahashi, E. In situ x-ray observation of the phase transformation of Fe<sub>2</sub>O<sub>3</sub>. *J. Phys.: Condens. Matter* **2005**, *17*, 269.

- (16) Ono, S.; Ohishi, Y. In situ X-ray observation of phase transformation in  $Fe_2O_3$  at high pressures and high temperatures. *J. Phys. Chem. Solids* **2005**, *66*, 1714–1720.
- (17) Bykova, E.; Dubrovinsky, L.; Dubrovinskaia, N.; Bykov, M.; McCammon, C.; Ovsyannikov, S. V.; Liermann, H.-P.; Kupenko, I.; Chumakov, A.; Rüffer, R. Structural complexity of simple Fe<sub>2</sub>O<sub>3</sub> at high pressures and temperatures. *Nat. Commun.* **2016**, *7*, 10661.
- (18) Boulard, E.; Guyot, F.; Menguy, N.; Corgne, A.; Auzende, A.-L.; Perrillat, J.-P.; Fiquet, G. CO<sub>2</sub>-induced destabilization of pyrite-structured FeO<sub>2</sub>H<sub>x</sub> in the lower mantle. *Natl. Sci. Rev.* **2018**, online, DOI: 10.1093/nsr/nwy032.
- (19) Huang, S.; Wu, X.; Qin, S. Ultra-high pressure phase transitions in  $FeS_2$  and  $FeO_2$ : implications for super-Earths' deep interior. *J. Geophys. Res.: Solid Earth* **2018**, 123, 277–284.
- (20) Bykova, E.; Bykov, M.; Prakapenka, V.; Konôpková, Z.; Liermann, H.-P.; Dubrovinskaia, N.; Dubrovinsky, L. Novel high pressure monoclinic Fe<sub>2</sub>O<sub>3</sub> polymorph revealed by single-crystal synchrotron X-ray diffraction studies. *High Pres. Res.* **2013**, 33, 534–545.
- (21) Staykov, A.; Téllez, H.; Akbay, T.; Druce, J.; Ishihara, T.; Kilner, J. Oxygen activation and dissociation on transition metal free perovskite surfaces. *Chem. Mater.* **2015**, *27*, 8273–8281.
- (22) Oganov, A. R.; Gillan, M. J.; Price, G. D. Structural stability of silica at high pressures and temperatures. *Phys. Rev. B: Condens. Matter Mater. Phys.* **2005**, *71*, 064104.
- (23) Zhu, S.-c.; Hu, Q.; Mao, W. L.; Mao, H.-k.; Sheng, H. Hydrogen-Bond Symmetrization Breakdown and Dehydrogenation Mechanism of FeO2H at High Pressure. *J. Am. Chem. Soc.* **2017**, *139*, 12129–12132.
- (24) Dudarev, S. L.; Botton, G. A.; Savrasov, S. Y.; Humphreys, C. J.; Sutton, A. P. Electron-energy-loss spectra and the structural stability of nickel oxide: An LSDA+U study. *Phys. Rev. B: Condens. Matter Mater. Phys.* **1998**, *57*, 1505.
- (25) Hu, Q.; Kim, D. Y.; Liu, J.; Meng, Y.; Yang, L.; Zhang, D.; Mao, W. L.; Mao, H.-k. Dehydrogenation of goethite in Earth's deep lower mantle. *Proc. Natl. Acad. Sci. U.S.A.* **2017**, *114*, 1498–1501.
- (26) Shim, S.-H.; Bengtson, A.; Morgan, D.; Sturhahn, W.; Catalli, K.; Zhao, J.; Lerche, M.; Prakapenka, V. Electronic and magnetic structures of the postperovskite-type Fe<sub>2</sub>O<sub>3</sub> and implications for planetary magnetic records and deep interiors. *Proc. Natl. Acad. Sci. U.S.A.* **2009**, *106*, 5508–5512.
- (27) Zhao, W.-N.; Zhu, S.-C.; Li, Y.-F.; Liu, Z.-P. Three-phase junction for modulating electron-hole migration in anatase-rutile photocatalysts. *Chem. Sci.* **2015**, *6*, 3483–3494.
- (28) Ziebarth, B.; Mrovec, M.; Elsässer, C.; Gumbsch, P. Interstitial iron impurities at grain boundaries in silicon: A first-principles study. *Phys. Rev. B: Condens. Matter Mater. Phys.* **2015**, *91*, 035309.
- (29) Badro, J.; Fiquet, G.; Struzhkin, V. V.; Somayazulu, M.; Mao, H.-k.; Shen, G.; Le Bihan, T. Nature of the high-pressure transition in Fe<sub>2</sub>O<sub>3</sub> hematite. *Phys. Rev. Lett.* **2002**, *89*, 205504.
- (30) Sheppard, D.; Xiao, P.; Chemelewski, W.; Johnson, D. D.; Henkelman, G. A generalized solid-state nudged elastic band method. *J. Chem. Phys.* **2012**, *136*, 074103.
- (31) Oganov, A. R.; Martoňák, R.; Laio, A.; Raiteri, P.; Parrinello, M. Anisotropy of Earth's D" layer and stacking faults in the MgSiO<sub>3</sub> postperovskite phase. *Nature* **2005**, *438*, 1142–1144.
- (32) Shang, C.; Liu, Z.-P. Stochastic surface walking method for structure prediction and pathway searching. *J. Chem. Theory Comput.* **2013**, *9*, 1838–1845.
- (33) Zhang, X.-J.; Shang, C.; Liu, Z.-P. Double-ended surface walking method for pathway building and transition state location of complex reactions. *J. Chem. Theory Comput.* **2013**, *9*, 5745–5753.
- (34) Qian, G.-R.; Dong, X.; Zhou, X.-F.; Tian, Y.; Oganov, A. R.; Wang, H.-T. Variable cell nudged elastic band method for studying solid-solid structural phase transitions. *Comput. Phys. Commun.* **2013**, 184, 2111–2118.

(35) Zhang, X.-J.; Liu, Z.-P. Variable-cell double-ended surface walking method for fast transition state location of solid phase transitions. *J. Chem. Theory Comput.* **2015**, *11*, 4885–4894.

- (36) Tschauner, O.; Kiefer, B.; Liu, H.; Sinogeikin, S.; Somayazulu, M.; Luo, S.-N. Possible structural polymorphism in Al-bearing magnesiumsilicate post-perovskite. *Am. Mineral.* **2008**, *93*, 533–539.
- (37) Zhu, S.-C.; Guan, S.-H.; Zhao, W.-N.; Liu, Z.-P. Atomic structure of heterophase junction from theoretical prediction. *Top. Catal.* **2015**, *58*, 644–654.
- (38) Liu, J.; Hu, Q.; Young Kim, D.; Wu, Z.; Wang, W.; Xiao, Y.; Chow, P.; Meng, Y.; Prakapenka, V. B.; Mao, H.-K.; Mao, W. L. Hydrogen-bearing iron peroxide and the origin of ultralow-velocity zones. *Nature* **2017**, *551*, 494.
- (39) Mao, H.-K.; Hu, Q.; Yang, L.; Liu, J.; Kim, D. Y.; Meng, Y.; Zhang, L.; Prakapenka, V. B.; Yang, W.; Mao, W. L. When water meets iron at Earth's core—mantle boundary. *Natl. Sci. Rev.* **2017**, *4*, 870–878.
- (40) Yuan, L.; Ohtani, E.; Ikuta, D.; Kamada, S.; Tsuchiya, J.; Naohisa, H.; Ohishi, Y.; Suzuki, A. Chemical Reactions Between Fe and H<sub>2</sub>O up to Megabar Pressures and Implications for Water Storage in the Earth's Mantle and Core. *Geophys. Res. Lett.* **2018**, *45*, 1330–1338
- (41) Hirose, K.; Sinmyo, R.; Hernlund, J. Perovskite in Earth's deep interior. *Science* **2017**, 358, 734–738.
- (42) Zhang, L.; Yuan, H.; Meng, Y.; Mao, H.-k. Discovery of a hexagonal ultradense hydrous phase in (Fe,Al)OOH. *Proc. Natl. Acad. Sci. U.S.A.* **2018**, *115*, 2908–2911.
- (43) Liu, J.; Dorfman, S. M.; Zhu, F.; Li, J.; Wang, Y.; Zhang, D.; Xiao, Y.; Bi, W.; Alp, E. E. Valence and spin states of iron are invisible in Earth's lower mantle. *Nat. Commun.* **2018**, *9*, 1284.
- (44) Liu, Y.; Oganov, A. R.; Wang, S.; Zhu, Q.; Dong, X.; Kresse, G. Prediction of new thermodynamically stable aluminum oxides. *Sci. Rep.* **2015**, *5*, 9518.